An All-Weather Observational Operator for Radiance Data Assimilation with Mesoscale Forecast Models

THOMAS J. GREENWALD, ROLF HERTENSTEIN, AND TOMISLAVA VUKIĆEVIĆ

Cooperative Institute for Research in the Atmosphere, Colorado State University, Fort Collins, Colorado

(Manuscript received 23 August 2001, in final form 16 January 2002)

ABSTRACT

Assimilating satellite radiance data under all weather conditions remains an outstanding problem in numerical weather prediction. This study develops an observational operator for use in radiance assimilation under both clear and cloudy conditions specifically for mesoscale models containing explicit microphysics. It is part of a larger research effort to build a 4D variational radiance assimilation system for optimal use of satellite data. The operator is suitable for radiance calculations at visible/infrared wavelengths and is adaptable to the different spectral characteristics of many types of narrowband satellite sensors. The new operator makes use of a gas extinction model and fast, multiple-scattering radiative transfer models, and relies on physical approximations for deriving cloud optical properties. One property, the asymmetry factor, is estimated through a new application of anomalous diffraction theory.

A test of the observational operator's ability to estimate cloudy radiances was performed by forecasting a continental stratus system using the Regional Atmospheric Modeling System and computing radiances at all channels of the *Geostationary Operational Environmental Satellite-9* imager. The forecasted radiances were found to reproduce very well the frequency distributions of observed cloudy radiances, particularly, the subtle temporal changes in the distributions that occurred between the early and late stages of development of the cloud system. These results are very encouraging and hold promise for future application of this observational operator in a full radiance assimilation system for satellite data across a wide range of wavelengths.

1. Introduction

Satellite data are playing an increasingly prominent role in numerical weather prediction (NWP). Infrared and microwave sounding data have brought improvements to moisture and temperature analyses (e.g., Eyre et al. 1993; English et al. 2000) while satellite cloud products have had similar positive impacts on the forecasting of clouds (e.g., Bayler et al. 2000). Despite these successes, an outstanding problem that remains in NWP is the difficult task of assimilating radiance data not only under clear conditions but cloudy as well.

While assimilating cloudy radiances may prove beneficial to weather forecasts and have fewer drawbacks than assimilating derived products (Eyre 1987), progress in this area has been rather slow. One reason is that global models have lacked the spatial resolution needed to resolve clouds and have only recently predicted physical cloud variables, which are preferred for an observational operator. Slow to develop as well have been physical cloud parameterizations for regional-scale forecast models. However, it is the ability to explicitly predict clouds at mesoscales that is the minimum requirement for fully exploiting the information content and mesoscale variability that satellite radiance data provide. Also contributing to this lack of progress to a certain extent has been the shortage of fast radiative transfer models for cloudy atmospheres. While many types of models do exist, the vast majority of them are impractical for data assimilation.

This study develops and verifies a practical general-purpose observational operator for computing visible and infrared radiances for use with mesoscale forecast models containing explicit microphysical schemes. The emphasis here is cloudy conditions. This work is the first step towards incorporating radiative transfer models into a 4D variational (4DVAR) system for the Regional Atmospheric Modeling System (RAMS) allowing, for the first time, the use of satellite radiance data under all weather conditions. A 4DVAR data assimilation algorithm for RAMS was recently developed at the Cooperative Institute for Research in the Atmosphere at Colorado State University (Vukićević et al. 2001). This algorithm includes the complete adjoint model for RAMS—enabling physical adjustments of cloud microphysical quantities. The new operator is validated through RAMS's forecast of a continental stratus system and comparison of the computed radiances to *Geostationary Operational Environmental Satellite-9* (*GOES-9*) imager data.

Corresponding author address: Dr. Thomas J. Greenwald, CIRA, Colorado State University, Fort Collins, CO 80523-1375.
E-mail: greenwald@cira.colostate.edu

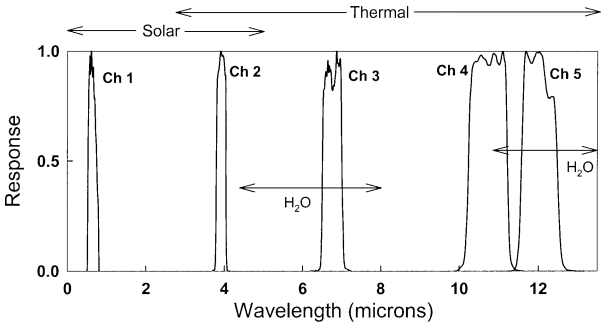

FIG. 1. Spectral regions detected by *GOES-9* imager channels 1–5. Radiation sources and regions of strong water vapor absorption are also indicated.

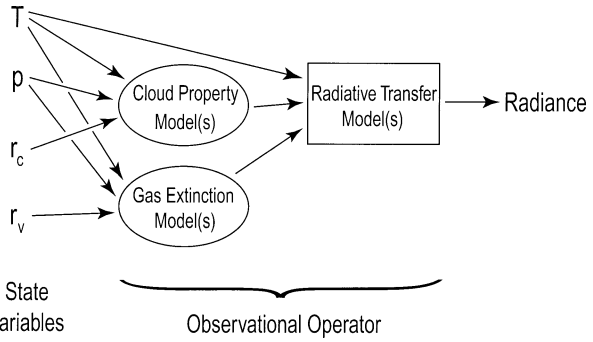

FIG. 2. Transformation of model state variables, temperature (T), pressure (p), cloud mixing ratio (r_c), and water vapor mixing ratio (r_v) into radiance via the observational operator.

The contents of this paper are as follows. The first two sections provide overviews of RAMS and the GOES imager. The next section outlines in detail the process of selecting appropriate models for the observational operator, which includes a new parameterization for one of the cloud optical properties. Next, a description of the case study is given followed by a summary of the RAMS's forecast of the stratus system. Section 7 presents results for a 3D large eddy simulation (LES) used to provide guidance in specifying droplet spectra information not predicted by RAMS and in assessing errors in visible radiance calculations. Verification of the observational operator is provided in the next section with concluding remarks in the final section.

2. Mesoscale model description

This study utilizes the well-known RAMS, which evolved from the Colorado State University cloud–mesoscale model described by Tripoli and Cotton (1982). RAMS is a nonhydrostatic primitive equation model that uses a $\sigma - Z$ terrain-following vertical coordinate (Tripoli 1986) and also has the capability to run in LES mode. Details regarding the model equations, vertical coordinate, grid structure, time differencing, and available parameterizations can be found in Pielke et al. (1992).

RAMS has several notable features. It includes the Land Ecosystem Atmosphere Feedback model, version 2 (LEAF-2), which treats storage and vertical exchange of water and energy in multiple soil layers, including effects of vegetation. Clouds and precipitation are explicitly represented via a microphysics parameterization that features a one-moment scheme for cloud liquid water (Walko et al. 1995) and a two-moment scheme for rain, aggregates, graupel, hail, snow, and pristine ice (Meyers et al. 1997). A more sophisticated bin microphysics parameterization is also available. Radiative fluxes are parameterized via a two-stream scheme developed by Harrington (1997).

3. GOES imager data

The imagers on the *GOES I-M* series of satellites (Menzel and Purdom 1994) have five channels that measure radiance in relatively narrow bands of the visible and infrared spectrum (see Fig. 1). They provide relatively high spatial resolution imagery (0.5 × 1.0 km, channel 1; 4 × 8 km, channel 2; and 2 × 4 km, channels 2, 4, and 5) every 15 min over most of the Northern Hemisphere. See Menzel and Purdom (1994) for details about these imagers. Calibration of the infrared channels (2–5) is performed aboard the satellite. Absolute calibration is estimated to be within 1 K. Channel 1 undergoes preflight calibration but has no onboard means of calibration. Studies indicate that this channel on *GOES-8* has degraded roughly 5.6%–7.6% each year since 1994 (Knapp and Vonder Haar 2000; Bremer et al. 1998). We chose here to use *GOES-9* imager measurements because at the time of the case study *GOES-9* had been in orbit less time than *GOES-8*, hence likely undergoing less degradation in channel 1. Based on the results of Bremer et al. (1998), we estimate the degradation in this channel is negligible.

4. Development of an all-weather observational operator

An observational operator transforms dynamical model state variables (such as cloud and vapor mixing ratio) into quantities with units of the observations, which in this case is radiance. This operator is often viewed as consisting of one model, namely a radiative transfer model. It is perhaps best to view the operator, however, as having several distinct parts (see Fig. 2). This is because radiative transfer models typically do not accept state variables directly (except, for instance, atmospheric temperature); rather, they require intermediate models or parameterizations that provide atmospheric gas and cloud properties that in turn depend on state variables. Our strategy is to construct a *general* operator applicable across visible and infrared wavelengths under all conditions, and which is based on

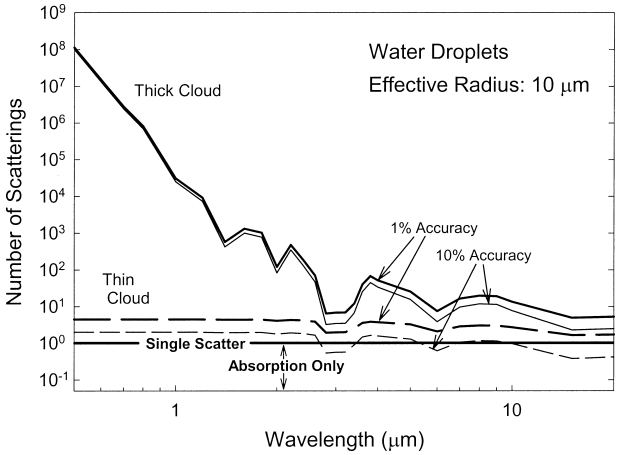

FIG. 3. Estimated number of photon scatterings needed to achieve 1% and 10% accuracy in radiance calculations at visible and infrared wavelengths for thin (optical depth of 0.5) and thick (optical depth of 30) clouds composed of water droplets. Molecular scattering and absorption are excluded.

physical approximations when possible. The key advantages of a general operator are that it more easily accommodates observations from new satellite instruments (particularly those with many channels) since it does not require creating entirely new models and, in addition, it can be quickly adapted to different hydrometeor types predicted by the mesoscale model.

a. Radiative transfer models

Strictly speaking, radiative transfer (RT) models represent the methods of solution of the monochromatic radiative transfer equation. For reasons of simplicity and practicality, only 1D RT models (i.e., vertical variation only) are considered for use in the observational operator. Also, cloud overlap, which must be dealt with in larger-scale forecast models, is ignored here since the mesoscale forecast model grid spacing is assumed to be relatively small.

Radiative transfer models are commonly used in assimilating clear sky infrared satellite data because under these conditions the atmosphere is purely absorbing–emitting where simple nonscattering RT models are applicable. However, scattering cannot be neglected for radiative transfer in cloudy atmospheres or in clear skies at solar wavelengths. This can be understood by examining the approximate number of scatterings that a photon at different wavelengths undergoes as it encounters cloud particles (Fig. 3). To achieve 1% accuracy in computed radiance for water clouds over a wide range of optical depths across all wavelengths (0.5–20 μm) in the absence of an atmosphere requires more than one scatter (i.e., single scatter) and in most cases many orders of scattering. Relaxing the accuracy to 10% allows the use of absorption-only (i.e., nonscattering) models, but only at wavelengths greater than about 10 μm and just for optically thin clouds. For realistic atmospheres in regions of strong gaseous absorption, however, scattering can be ignored regardless of wavelength. But while in window regions where gaseous absorption also reduces the number of photon scatterings, multipl-scattering RT models must be used at visible wavelengths and are generally needed at shorter IR wavelengths in order to achieve reasonable accuracy in radiance calculations under many cloud conditions.

Selecting the best RT model in terms of accuracy and speed for an observational operator also depends on the type of radiation source. For instance, thermal-only sources occur for wavelengths greater than about 3 μm and because the angular scattering characteristics for particles at these wavelengths are relatively smooth, far simpler multiple-scattering RT models that use the asymmetry factor g (proportional to first moment of the scattering phase function[1]) may be used. These include two-stream methods, which reduce the radiation's angular dependence to one direction (stream) up and one down. These methods are very fast and have been shown to achieve accuracies in terms of equivalent blackbody temperature of less than 1.5–2 K for a wide range of cloud conditions (Deeter and Evans 1998). A two-stream model is used here for computing radiances in both clear and cloudy atmospheres based on the Eddington approximation (e.g., Deeter and Evans 1998) and uses Delta-M scaling to improve radiance calculations for highly peaked phase functions (Wiscombe 1977).

Computing cloudy radiances for a solar source (wavelengths $<\sim 5$ μm) is more challenging because the angular scattering patterns are more complicated and thus require more angular resolution (or streams) to resolve the radiance field. Traditional multistream methods are usually based on either eigenvalue approaches (e.g., DISORT − DIScrete Ordinate Radiative Transfer; Stamnes and Swanson 1981) or doubling–adding (DA)[2] methods (Grant and Hunt 1969; Wiscombe 1976). However, neither DISORT nor existing DA methods are suitable for a data assimilation system because they are too computationally inefficient. Recent advancements, however, have been made through hybrid numerical methods of solution. One method, the Spherical Harmonics Discrete Ordinate Method (SHDOM; Evans 1998), makes use of both a multistream (discrete ordinate) and a spherical harmonic characterization of the angular radiance field in a successive order of scattering-type approach. The advantage of using both types of representations is that transforming the source function between spherical har-

[1] The scattering phase function describes the full directional characteristics of single-scattered radiation.

[2] The DA method gets its name from numerical integration of the multiple scattering integral through *doubling* of homogeneous atmospheric layers and *adding* of nonhomogeneous layers. The doubling algorithm is most efficient for optically thinner atmospheres, requiring only n steps to integrate across a layer of thickness $2^n\Delta\tau$, where $\Delta\tau$ is an infinitesimally thin optical depth.

monics and discrete ordinates is actually faster than solving the problem with discrete ordinates alone (Evans 1998). SHDOM was initially built as a fast model for multidimensional radiative transfer but is used here in 1D. Because it is an order of scattering method, the number of iterations increases for optically thicker clouds and with increasing single-scatter albedo.[3]

Along with its flexibility in controlling accuracy versus speed, SHDOM has other important advantages and features that make it highly desirable for a data assimilation system. A spherical harmonics representation of the source function allows for higher accuracy with fewer streams, thus providing additional increases in speed. A convergence acceleration feature also reduces the number of iterations. In addition, SHDOM can accommodate more complicated scattering phase functions (such as Lorenz–Mie) without much additional computational burden, unlike other approaches.

b. Cloud property models

Single-scatter (or optical) properties of clouds are one of the crucial links between model state variables and RT models. The properties that scattering-based RT models require are the extinction coefficient, scattering phase function, and single-scatter albedo. Since rigorous approaches to computing these properties, such as Lorenz–Mie theory, are in most cases impractical, alternative methods must be developed. Our strategy is to employ physical approximations, which eliminates the need for developing ad hoc fitting functions that become cumbersome when dealing with different hydrometeor types and satellite sensors containing many spectral channels. Rapid and reasonably accurate calculation of these cloud properties is possible using anomalous diffraction theory (ADT; van de Hulst 1981). ADT assumes that particles are large compared to wavelength of the incident radiation (allows for ray tracing) and have refractive indices close to one (minimizes refraction of ray). Mitchell (2000) incorporated parameterizations of internal reflection–refraction, photon tunneling, and edge diffraction into ADT to make it applicable over a larger range of conditions. This modified form of ADT (MADT) is used in this study to compute the extinction coefficient and single-scatter albedo. Comparisons of MADT to Lorenz-Mie theory across the visible to infrared show that errors are less than 10% for droplet effective radii between 5 and 30 μm (Mitchell 2000).

Given that the microphysical parameterization predicts at most 2 moments of the particle size distributions, that is, mixing ratio and number concentration, a form of the distribution must be assumed in order to carry out these calculations. We use the well-known gamma distribution

$$N(D) = N_o D^{\nu} e^{-\Lambda D},$$

where D is the particle diameter and N_o, ν, and Λ are adjustable parameters. Here, N_o and Λ are implicit functions of mixing ratio and number concentration (see Mitchell 2000), while ν is related to the distribution width. Nonspherical particles, such as aggregates, graupel, hail, snow, and pristine ice, may be considered by choosing the appropriate projected area and mass-dimension relationship (Mitchell 1996), density, and refractive index. In summary, MADT requires the following diagnostic parameters: wavelength of observation, particle density, particle complex refractive index, and ν; prognostic parameters include cloud mixing ratio, particle number concentration, atmospheric temperature and pressure (the latter two are needed to convert mixing ratio to mass per unit volume).

The third optical property we must consider is the scattering phase function. Generally speaking, use of g alone is sufficient at infrared wavelengths; however, at solar wavelengths the full phase function must be specified. The analytic Henyey–Greenstein (HG) phase function was chosen because it is a smooth function that requires fewer terms in its expansion and thus significantly reduces RT model execution time.[4] The Legendre Polynomial expansion of the HG phase function is

$$P(\Theta) = \sum_{\ell=0}^{N} (2\ell + 1) g^{\ell} P_{\ell}(\Theta),$$

where Θ is the scattering angle and l is the order of Legendre Polynomial P_l. The HG phase function, unfortunately, does not capture the strong forward peak and backscattering feature seen in the Lorenz–Mie phase function. Reflectance errors due to these deficiencies are addressed in section 7.

An estimate of g is obtained here by applying ADT. Details concerning theory and computational aspects are given in appendix A. Computing g requires the same input as MADT except for pressure and temperature. Overall, ADT performs best at longer wavelengths (6.77 μm and greater) under most conditions with errors under 2% (Fig. 4), but expectedly breaks down for droplets much smaller than wavelength (the Rayleigh scattering limit). At 3.92 μm, errors are generally less than 10% in the range of effective radii expected for most cloud droplets. Increasing errors for larger effective radii are due to a breakdown of ADT in the geometric optics limit (droplets very large compared to wavelength). At visible wavelengths (0.629 μm) these errors are even more dramatic (sometimes greater than 80%) and show that ADT is useful only for the smallest droplets (<4 μm). Incorporating a parameterization of internal reflection–refraction at these wavelengths may be possible (e.g., Mitchell 2000) but is beyond the scope of this

[3] Single-scatter albedo is the probability that a photon is scattered.

[4] More complicated phase functions, such as Lorenz–Mie, at visible wavelengths usually require, depending on particle size, several 100 or more polynomial terms to be adequately represented. Execution time is related to the number of streams in the RT model, which is proportional to the number of terms needed.

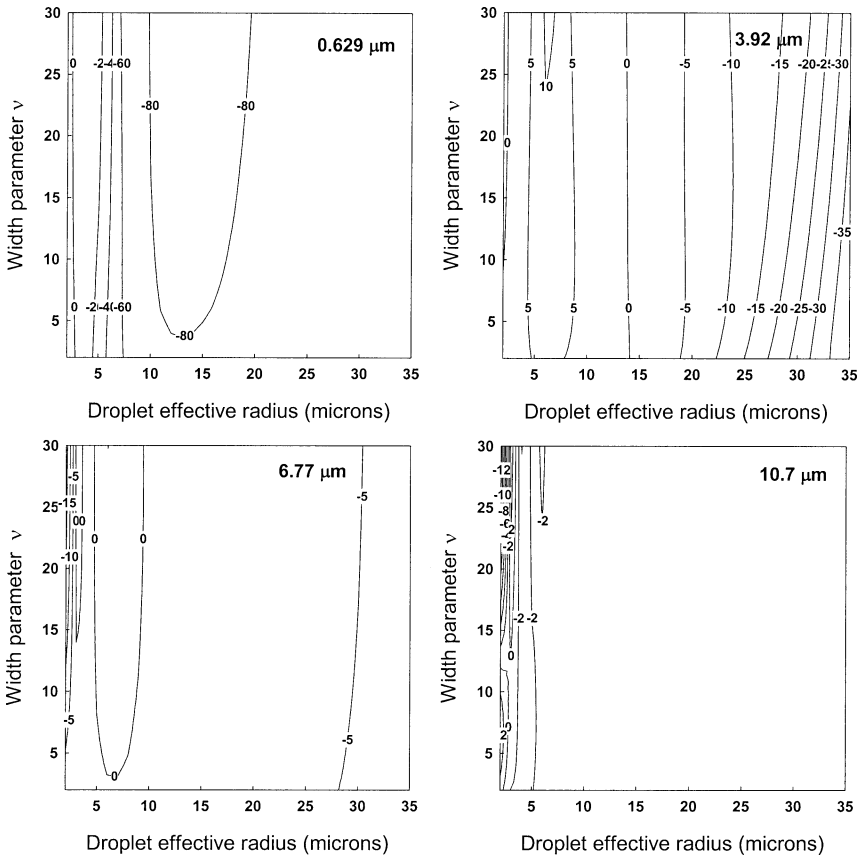

FIG. 4. Errors (%) in anomalous diffraction theory estimates of the asymmetry factor as compared to Lorenz–Mie theory as a function of gamma distribution width parameter ν and effective radii at selected wavelengths.

study. As a replacement, an ad hoc empirical parameterization for g is used in applying the observational operator to the GOES imager visible channel (see appendix B).

c. Gas extinction model

Accounting for gaseous absorption requires the use of simplified models since detailed line-by-line (LBL) calculations at visible and infrared wavelengths are impractical. Single-band models are generally of sufficient accuracy for modeling gas absorption across relatively narrow spectral band satellite measurements. The widely known single-band model called OPTRAN (Optical Path TRANsmittance) developed by McMillin et al. (1995a,b) is applied here, and is currently used in at least one data assimilation system (e.g., Derber and Wu 1998). In OPTRAN, regression coefficients are computed for the transmittance (in this case, the effective absorption coefficient) at fixed values of the absorber optical depth, where the predictors are temperature, pressure, and their various combinations. OPTRAN depends on the model state variables of atmospheric temperature, pressure, and water vapor mixing ratio.

When applied to all channels of the *GOES-9* imager and compared to LBL calculations in terms of equivalent blackbody temperatures (Table 1), OPTRAN mean errors were less than about 0.2 K with a maximum error of 0.85 K. Soden et al. (2000) showed, however, that OPTRAN exhibits an overall bias of +1.1 K for radiance calculations at GOES imager channel 3 over a wide range of atmospheric conditions. For channel 1, the absolute errors in terms of optical depth are about 1% in comparison to LBL calculations. Applying OPTRAN to other satellite sensors requires the generation of new regression coefficients depending on the spectral characteristics of the sensor's channels.

TABLE 1. OPTRAN errors in terms of equivalent blackbody temperature for the *GOES-9* Imager relative to line-by-line calculations.

Channel	Mean error (K)	Std error (K)	Max error (K)
2	0.0183	−0.000203	−0.0490
3	−0.212	0.192	−0.846
4	−0.00656	0.0273	0.110
5	0.00603	0.0298	−0.116

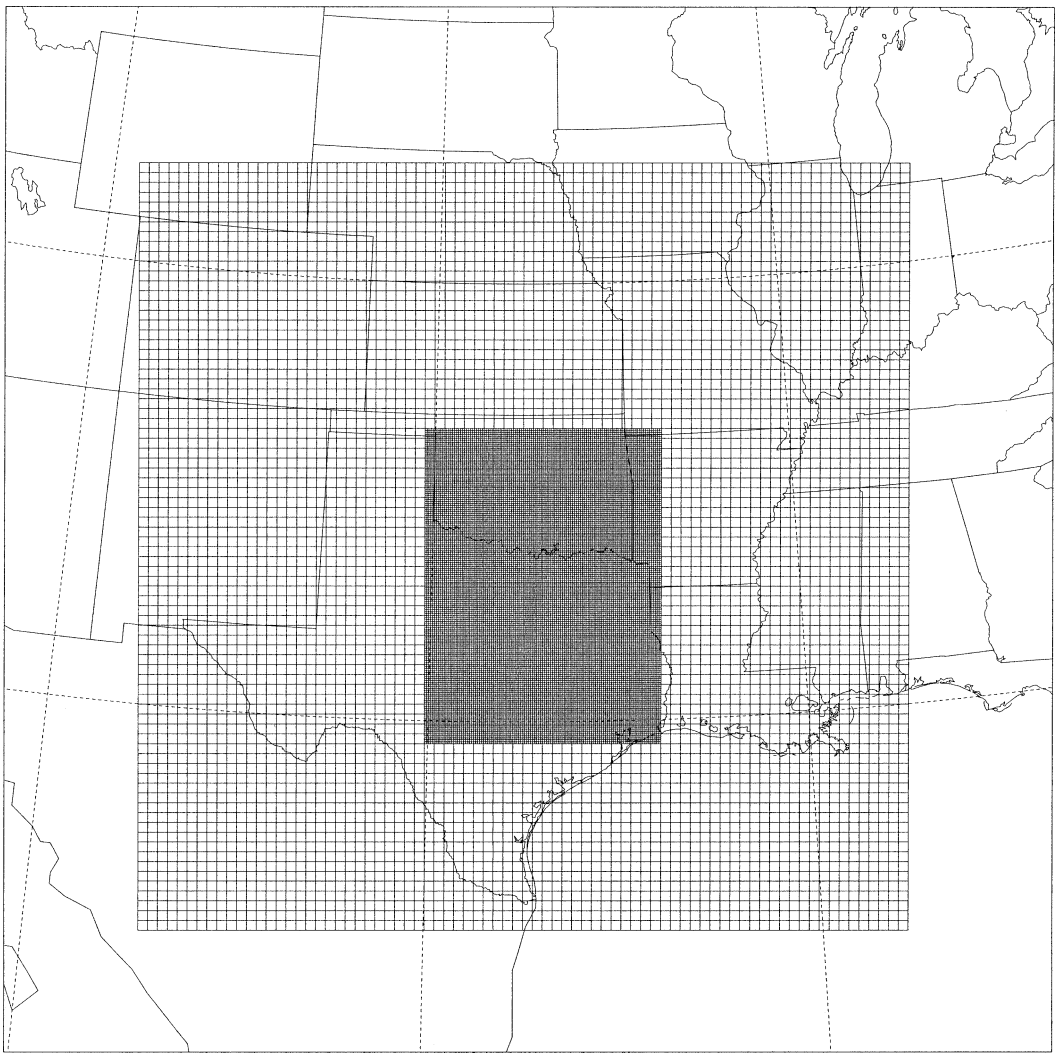

FIG. 5. RAMS grid configurations used in this study.

5. Case study

Forecast of a continental stratus system was chosen to help evaluate the newly developed observational operator coupled to a mesoscale model. The cloud system developed over a broad area of Texas and Oklahoma on 2 May 1996. The 500-mb flow in this region at 1200 UTC was generally zonal at about 20 m s^{-1} with a weak short-wave trough just to the west. Surface analyses indicated moist southerly flow over eastern Texas, with much drier air in the western part of the state. At 1200 UTC a warm front was also situated on the Texas–Oklahoma border with cooler, drier air and light south-southeasterly winds in Oklahoma. No precipitation was reported from surface observations or radar in association with the warm front.

Satellite data showed that by sunrise on 2 May (approximately 1200 UTC), widespread stratus had already developed. The cloud system was near its greatest spatial extent at about 1500 UTC. Three hours later the cloud system's spatial extent began to noticeably shrink and by 2100 UTC it had greatly dissipated, with a region of broken stratocumulus in northeast Texas. Cloud coverage again increased over Texas towards sunset.

6. Mesoscale model forecast

The forecast was performed with two grids using the interactive-nesting capability of RAMS. The coarse grid had 80 × 80 points, with a spacing of 25 km, while the fine grid was 122 × 162 points at 5-km spacing (see Fig. 5). The fine-grid spacing was chosen to coincide approximately with the spatial resolution of GOES data. Vertically, we used 50 levels with constant spacing of 50 m to the 1200-m level (to better resolve the low-level cloud), then stretching gradually to a spacing of 1200 m at the top of the model domain (~18 km) on both coarse and fine grids. Standard land-use datasets, that is, topography, vegetation, and sea surface tem-

TABLE 2. RAMS surface air temperature and dewpoint differences from selected surface station observations for the 12-h forecast.

Station #	ΔT (K)	ΔT_d (K)	Latitude	Longitude
1	−0.83	−1.2	29.97°N	95.35°W
2	1.6	1.2	32.47°N	93.82°W
3	−1.6	−0.52	29.53°N	98.47°W
4	−1.2	−0.37	31.62°N	97.23°W
5	−2.9	−0.78	32.90°N	97.03°W
6	−1.4	−1.8	32.42°N	99.68°W
7	−1.6	−0.43	35.33°N	94.37°W
8	0.67	0.53	33.97°N	98.48°W
9	3.5	−1.1	35.40°N	97.60°W
10	−3.8	1.2	36.20°N	95.90°W
Mean	−0.76	−0.33		

perature, are interpolated onto the model grid, while a horizontally homogeneous initialization of soil moisture is used across the entire domain. The model atmosphere was initialized using NCEP–NCAR reanalysis data as background; available standard rawinsondes and surface observations were then interpolated onto the model grid.

The forecast started at 0000 UTC on 2 May and ran for 24 h. A cluster of eight 500-MHz processors was used, which allowed the simulation to run almost real time. Overall, RAMS had reasonable skill in forecasting the areal extent of the cloud system and in the timing of its development and dissipation, but was unable to produce thick clouds in eastern Oklahoma as observed from satellite. This is likely attributed to an underestimation of boundary layer moisture in that region. Boundary layer moisture errors are most evident in a comparison of the total precipitable water (TPW) 18-h forecast and the 1800 UTC NCEP reanalysis (not shown). NCEP analysis indicated high TPW values over much of the eastern half of the domain, as would be needed for forming the very thick cloud observed over Oklahoma. In contrast, the highest forecasted values of TPW were confined to central Texas. This result is also consistent with a comparison of 12-h forecast surface temperature and dewpoint with surface observations at 10 stations located throughout the domain, which showed that overall the forecast tended to be too cool and too dry (Table 2). Furthermore, a sounding taken from the Morris, Oklahoma ARM (Atmospheric Radiation Measurement) site at 1735 UTC (not shown) indicated that the forecasted vapor mixing ratios in the inversion-capped mixed layer were about 14% too low. RAMS's underestimation of the boundary layer precipitable water was not only limited to the 18-h forecast. A time series of TPW from the ground-based microwave radiometer at Morris shows that the forecast consistently underestimated TPW (Fig. 6), suggesting perhaps an initialization error in the forecast.

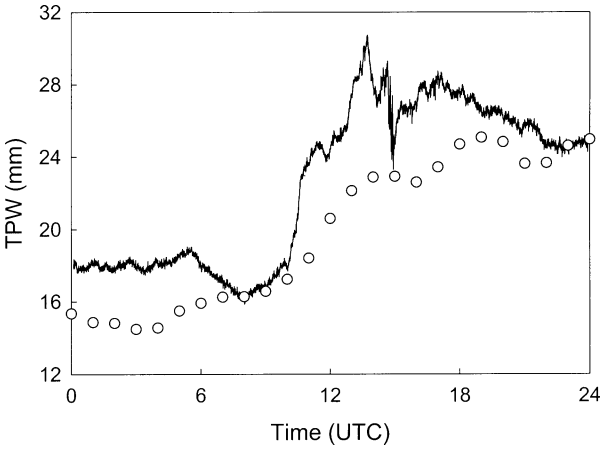

FIG. 6. Time series of total precipitable water (TPW) for ground-based microwave radiometer vs RAMS forecast for 2 May 1996 at Morris, OK.

7. Evaluating errors using large eddy simulations

A large eddy simulation is a useful diagnostic tool for this study in several respects. First, it is helpful in specifying microphysical parameters that are not predicted by the mesoscale model but are needed by the observational operator. It also can estimate errors in approximations used in the observational operator and is useful in investigating subgrid-scale effects on solar radiances. Because the grid spacing used in typical forecasts is too coarse to resolve the individual large eddies of the cloud system, these unresolved features could ultimately affect the radiance field. It is important to keep in mind that this effort is not an attempt to simulate the actual cloud system that occurred during the case study period. Rather, the results are used for sensitivity purposes on a similarly structured cloud under similar environmental conditions.

a. Model configuration and results

RAMS was run with a domain size of 100 × 100 points at 200-m horizontal spacing with 50 points in the vertical at 50-m spacing. A grid spacing of 200 m has been found to be adequate in resolving turbulent eddies in stratus. Cyclic lateral boundaries were used with an absorbing layer active at the top six model levels. A bin microphysics scheme (Feingold et al. 1996) was implemented with 34 bins ranging in diameter from 3.25 μm to 8 mm.

Initialization was the 1730 UTC Morris, Oklahoma, sounding on 2 May 1996. Because the sounding was slightly subsaturated at levels just below the inversion and at this time GOES visible imagery indicated a pronounced cloud over the launch site, the sounding was moistened somewhat at these levels. Several 2D LESs were run before committing to the 3D LES and found that the simulations were relatively insensitive to the amount of moistening in the initial sounding and soil moisture profile.

The LES was run for 4 h, at which time the model cloud appeared to reach a quasi-steady state (Fig. 7) and

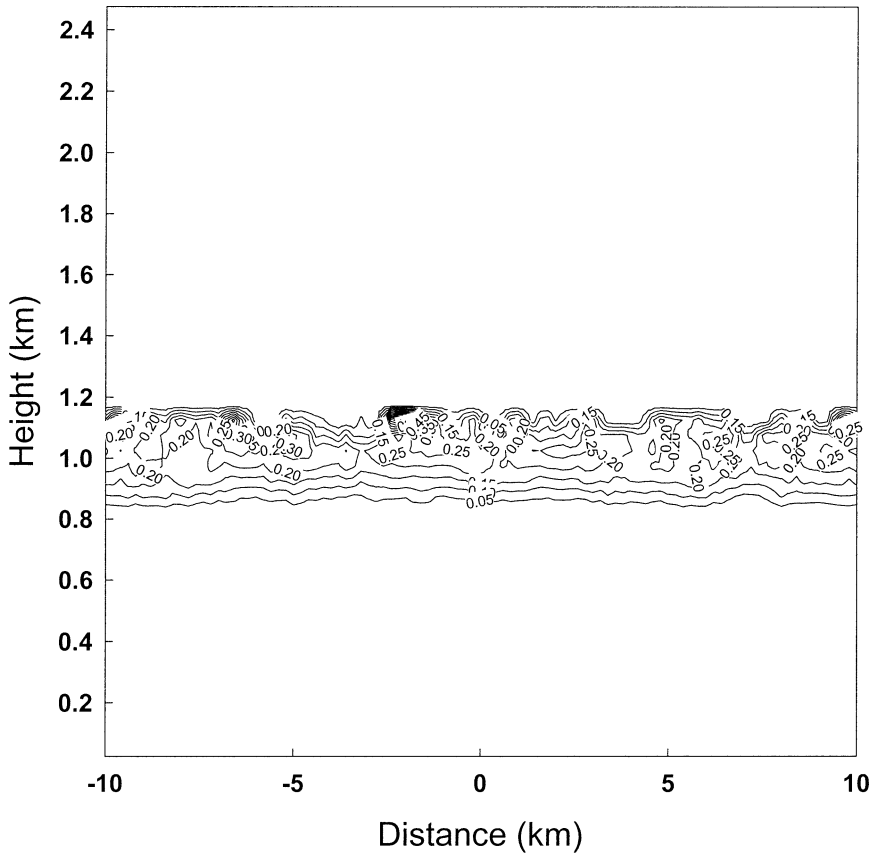

FIG. 7. Cross section of the large eddy simulation for cloud water mixing ratio (g kg^{-1}).

completely filled the domain. When averaged over the entire domain, the vertical structure of the number concentration and liquid water content generally increased with increasing height (Fig. 8) as often observed (e.g., Miles et al. 2000). The overall statistics are shown in Table 3. The mean and standard deviation of the number concentration compared very well to 288 $\pm$ 159 cm^{-3} based on a summary of many observational studies of continental stratus (Miles et al. 2000), providing added assurance that the LES has produced a cloud with reasonable microphysical characteristics.

With knowledge of the complete droplet spectra the shape or width of the size distribution may be determined, which is an unknown in the observational operator. This parameter (ν) was estimated by fitting spectra to a gamma distribution through least squares regression. In Fig. 8, ν generally increases with height, which reflects a narrowing of the size distribution. This narrowing near cloud top is indicative of long-wave cooling (Harrington et al. 2000).

b. 3D radiative transfer results

The LES was also used to investigate subgrid-scale effects on visible reflectances. To accomplish this we implemented SHDOM in 3D mode. Memory resources can become very large for these calculations; therefore, the experiment was limited to the southwest quadrant of the domain (10 km $\times$ 10 km in size). Because the goal is to quantify relative effects, Rayleigh scatter and gaseous absorption were neglected for simplicity.

First, Lorenz–Mie calculations at 0.63 μm were performed to obtain optical properties for each cloud droplet spectrum in the 3D field. Reflectance fields (200-m grid spacing) were computed for different solar geometry and zenith angles (Table 4) and then averaged spatially to 5 km to mimic the grid spacing used in the forecast. These grids served as ''truth'' reflectance fields from which errors were computed.

Next, the LES microphysical fields were spatially averaged to 5 km and Lorenz–Mie calculations were executed on these mean droplet spectra. Reflectance fields were then generated using SHDOM in 1D mode. Calculations were also done using the HG phase function in place of the Lorenz–Mie phase function in order to assess the errors in this approximation. Results show (Table 4) for a wide range of conditions that when using the Lorenz–Mie scattering phase function, errors due to subgrid-scale effects appear to be quite small (less than a few %) at least for this type of cloud system under overcast situations. It should be emphasized, however,

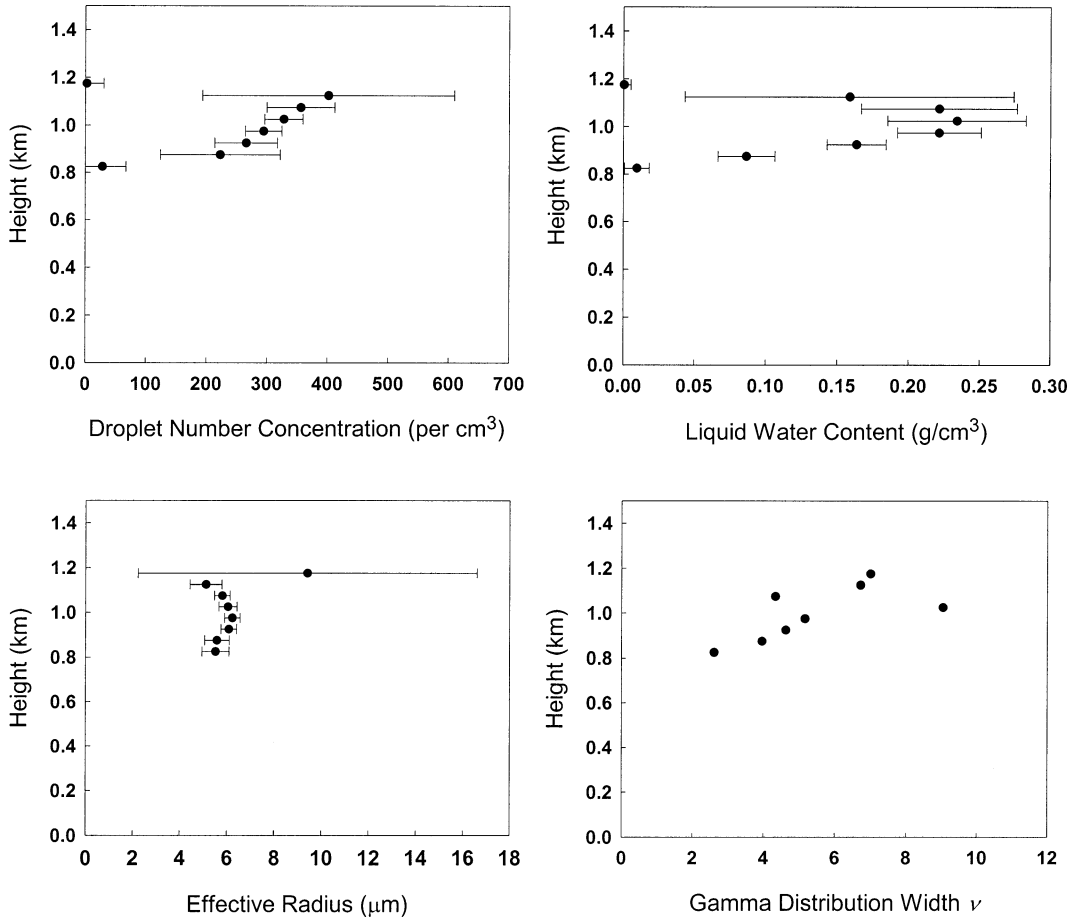

FIG. 8. Statistics (mean and std dev) of the large eddy simulation for droplet number concentration, liquid water content, and droplet effective radius as a function of height. Also shown is the mean width ν of the droplet spectra fitted to a gamma distribution.

that far larger errors would be expected for broken cloud fields.

Use of the HG phase function produced errors that depend greatly on the relative solar-observation geometry. This is because the HG phase function has a weaker, broader forward scatter peak relative to Lorenz–Mie theory and lacks the backscattering peak. In conditions where backscattering predominates, the HG phase function underestimates reflectance, with errors ranging from −9% to −23%. For more forward scattering conditions the tendency is for the HG phase function to overestimate the reflectance (9%–17%) because of its broader forward scattering peak. For a high sun (20° zenith angle) and a small observation zenith angle (20°) the errors become negative in all cases because under these conditions the solar radiation is primarily backscattered, regardless of the relative sun-observation azimuth angle.

TABLE 3. Overall statistics for LES in terms of droplet number concentration (N), liquid water content (LWC), and effective radius (r_e). Also shown are ν values obtained through a fit of the droplet spectra to a gamma distribution.

	Mean	Std dev
N (# cm^{-3})	246.8	160.3
LWC (g m^{-3})	0.142	0.100
r_e (μm)	6.10	2.46
ν	5.43	1.91

8. Application to the GOES imager

a. Observational operator setup

Preparing the observational operator's input and specifying various diagnostic parameters require further explanation. Table 5 summarizes the input used for the RT models. The number of streams in SHDOM was chosen as a compromise between speed and accuracy. On average, convergence was achieved in about 15–20 iterations for optically thick cloudy atmospheres. In clear sky conditions SHDOM runs much faster (about 5–12X faster) owing to smaller optical depths and only three

TABLE 4. Mean domain errors in 0.63–μm reflectances using spatially averaged microphysics and comparing Lorenz–Mie and Henyey–Greenstein (HG) scattering phase functions for different solar geometry and observation zenith angle (θ).

Solar zenith angle (deg.)	Relative azimuth angle* (deg)	$\theta = 20°$ Lorenz–Mie (%)	$\theta = 20°$ HG (%)	$\theta = 50°$ Lorenz–Mie (%)	$\theta = 50°$ HG (%)	General description
20	0	−1.6	−23	−2.3	−12	Backscatter
	90	−2.3	−6.3	−2.6	1.5	Intermediate
	180	−2.2	−5.5	−2.5	9.1	Forward scatter
60	0	−0.07	−9.3	1.5	−21	Backscatter
	90	−0.41	9.9	1.3	13	Intermediate
	180	−0.12	17	3.7	16	Forward scatter

* Azimuth angle between the sun and observation.

phase function expansion terms required for Rayleigh scatter.

RAMS's top level only reaches to about 18 km, so it was necessary to add several levels to the atmospheric profiles input to the observational operator. To include ozone, five levels at 21.4, 27.85, 37.7, 50, and 60 km were added based on a climatic midlatitude summer profile. Another atmospheric level at the surface (the lowest level was 25 m above ground level) was also added by extrapolating temperature, pressure, and water vapor mixing ratio to 0 m assuming a lapse rate of 6.5 K km^{-1}. Thus, a total of 56 levels was used.

Input values used for the MADT and ADT asymmetry factor models are provided in Table 6. Because only mixing ratio is predicted for liquid droplets, the droplet number concentration was set to a constant 1.7×10^8 number kg^{-1} (depending on air density, equivalent to about 187 cm^{-3}). It was found that specifying the mean concentration obtained from the LES results produced water droplets whose mean sizes were unreasonably small. Thus, a smaller value was used but still within the modeled and observed range of variability. The gamma distribution width parameter ν was set to 6, which is based on the average of the top three levels in Fig. 8.

b. Verification against GOES-9 imager data

The observational operator was used to produce 2D radiance fields over the fine-grid domain at 1500 and 2100 UTC using RAMS forecast state variables of pressure (more precisely the Exner function), potential temperature, and water vapor and cloud mixing ratio (Fig. 9). These two time periods best illustrate the evolution of the cloud system but also contrast two different solar geometries, where solar radiation seen by the GOES imager is more forward scattered at 1500 UTC and more backscattered at 2100 UTC. Channel 1 (visible) results are expressed in terms of reflectance, while all other channels are converted to equivalent blackbody (EBB) temperatures for easiest interpretation. For reference, a summary of the imager's information content and the qualitative sensitivity of these observations to the state variables are given in Table 7.

The forecasted visible reflectances in cloudy regions compare favorably to observations in terms of magnitude, though are biased low about 10%, a consequence perhaps of smaller cloud mixing ratios generated by RAMS and/or the crude assumptions regarding the scattering phase function. Also, the finer-scale features of the cloud system are not captured even though the model grid spacing is comparable to the resolution of the ob-

TABLE 5. Characteristics of and input values used for radiative transfer models in computing radiances at *GOES-9* imager channels. Boundary conditions are surface albedo (α_s), surface temperature (T_s), and surface emissivity (ε_s). Number of streams is given for zenith angle (zen) and azimuth angle (azm) space. Here, SH stands for spherical harmonics, accel is the convergence acceleration feature, and δ-M is Delta-M scaling. Rayleigh scatter is included in SHDOM for channel 1 calculations.

Model	No. streams Zen	No. streams Azm	Solution-related criteria: Adaptive grid?	SH accuracy	Solution accuracy[a]	Accel?	δ-M?	Boundary conditions: Ch. 1 α_s	Ch. 2 α_s	Ch. 2 T_s	Ch. 3–5 ε_s	Ch. 3–5 T_s
SHDOM	14	14	Yes	3×10^{-3}	10^{-3}	Yes	Yes	Model[b]	0.96[c]	Soil[d]	—	—
Two-stream	2	—	—	—	—	—	Yes	—	—	—	0.98	Soil[d]

[a] A unitless measure defined as root-mean-square (rms) difference in successive source function calculations normalized by rms of the source function.
[b] For grassland and solely a function of solar zenith angle (Sun-Mack et al. 1999).
[c] Smith et al. (1999).
[d] Temperature of upper 5 cm of soil layer in LEAF-2.

TABLE 6. Input values used for anomalous diffraction theory and radiative transfer calculations for *GOES-9* imager channels. Mean wavelength (λ_m) and droplet refractive indices (real part n_r and imaginary part n_i) are weighted by instrument response function (see Fig. 1) and solar spectrum for channels 1 and 2.

Channel	λ_m (μm)	n_r	n_i
1	0.629	1.33	2.86×10^{-8}
2	3.92	1.35	4.07×10^{-3}
3	6.77	1.32	3.62×10^{-2}
4	10.72	1.17	0.0834
5	12.01	1.13	0.204

servations. This is mainly because the effective resolution of model simulations is typically 4Δx, where Δx is the model grid spacing (Pielke et al. 1997).

Forecasted infrared window temperatures (channels 4 and 5) indicate a warm (i.e., low-level) cloud, as expected, throughout most of the domain (Fig. 9). The equivalent blackbody temperatures (EBBTs) for channel 5 are slightly colder relative to channel 4 due to somewhat stronger water vapor absorption, a behavior seen in the forecasted EBBTs as well. However, notable large discrepancies at these wavelengths and for channel 2 are seen in clear regions, especially in the western part of the domain. This resulted from RAMS's inability to correctly forecast large diurnal swings in soil temperature that occurred in this specific case. In the 21-h forecast, errors were as high as 20 K. The degree of soil warming is controlled greatly by the initialization of soil moisture in the surface model. Initial soil moisture was likely incorrectly specified but was not explored in this study because the focus was on cloud modeling.

At 6.7 μm (channel 3), the forecast does a remarkable job of reproducing the spatial patterns of the observed EBBTs (Fig. 9) although the forecast tends to be biased warm (i.e., too dry), sometimes as high as 5 K. Combined biases in OPTRAN and the two-stream RT model are anticipated to be no more than about 2 K. The remaining differences suggest an initialization error in humidity in the upper troposphere.

A more quantitative comparison is facilitated through frequency histograms in cloudy-only regions (Fig. 10). Good agreement is confirmed at the 15-h forecast (1500 UTC) where both modeled and observed distributions are skewed with maxima at high reflectance, a clear signature of a very thick, extensive cloud. At 21 h into the forecast, the observations show a shift to lower, more uniformly distributed reflectances that indicates the more broken and less organized nature of the cloud system at this time. At 1500 UTC both forecast and observations indicate clouds with an EBBT of 285 K on average with little variation (see Fig. 10), demonstrating RAMS has done well in forecasting cloud height and boundary layer temperature and humidity structure. At 2100 UTC the forecast replicates the subtle warming of the cloudy EBBTs and broadening of the EBBT frequency distribution as seen in the observations.

Radiances at 3.9 μm (channel 2) are unique in that they include the combined effects of scattered solar radiation by cloud particles and thermal emission (see Fig. 1). Because they are in a spectral region where liquid and ice absorption occurs, 3.9-μm radiances provide key information about mean particle size, unlike the other channels, and thus are more sensitive to details in the particle spectra. In cloudy-only regions (Fig. 10), the 15-h forecast EBBTs are biased lower (about 4 K) than observations. At 2100 UTC the observed EBBTs increase by more than 5 K due partly to increased thermal emission but mainly to a 28% increase in incoming solar flux (as compared to 1500 UTC). For the 21-h forecast the modeled EBBTs are slightly higher (about 2–3 K). These errors are likely associated with the scattered solar component since thermal emission (as reflected in the channel 4 comparisons) appears to be well predicted. Specifically, these errors are most likely traced to the limitation of predicting only one moment of the droplet size distribution. Reducing the number concentration by 40% was found to decrease the EBBT by roughly 3 K, large enough to account for the differences seen between the 21-h forecast and observations (Fig. 10).

9. Conclusions and future directions

A new observational operator has been assembled for computing radiances at visible–infrared wavelengths

TABLE 7. Information content provided by the GOES imager and the relative sensitivity of model state variables to the measurements. Here, T is temperature (both atmosphere and soil), p is pressure, N is particle number concentration, r_c is cloud mixing ratio, and r_v is water vapor mixing ratio.

Channel	Description	Primary information	Sensitivity to state variables	
			Stronger	Weaker
1	Visible	• Cloud optical depth • Surface albedo	r_c	T, p, r_v, N
2	Near-infrared	• Mean cloud particle size • Surface albedo and skin temperature	r_c, N, T	p, r_v
3	IR water vapor	• Upper-tropospheric humidity	r_v	T, p, r_c, N
4	IR window	• Cloud-top temperature • Surface skin temperature	r_c, T	p, r_v, N
5	IR window/vapor	• Cloud-top temperature • Surface skin temperature • Boundary layer humidity	r_c, r_v, T	p, N

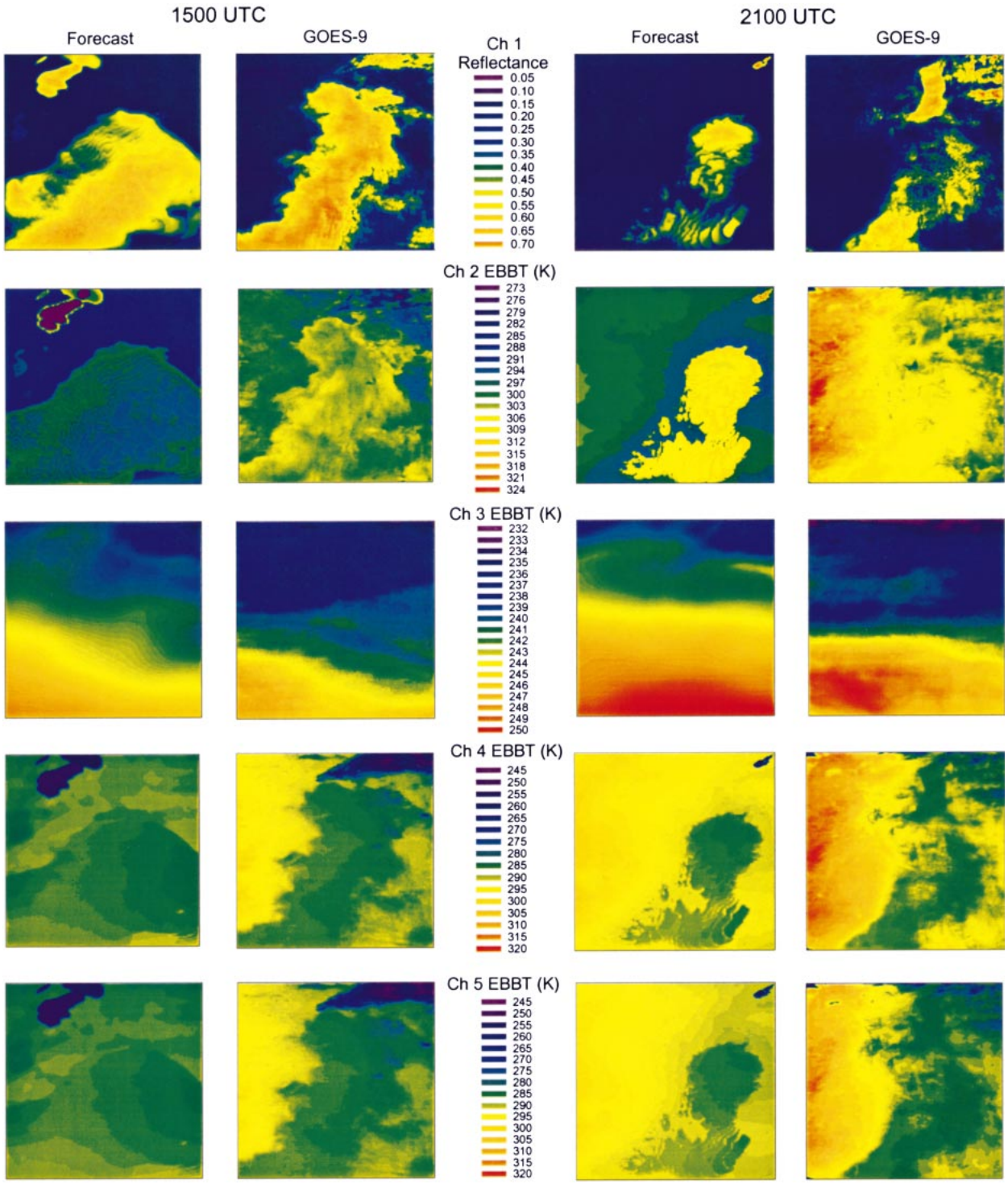

FIG. 9. Radiance fields for the nested grid 2 May 1996 at 1500 UTC (left pairs of panels) and 2100 UTC (right pairs of panels) comparing forecasts and *GOES-9* imager measurements at all five channels. Channels 2–5 are expressed in terms of equivalent blackbody temperature (EBBT).

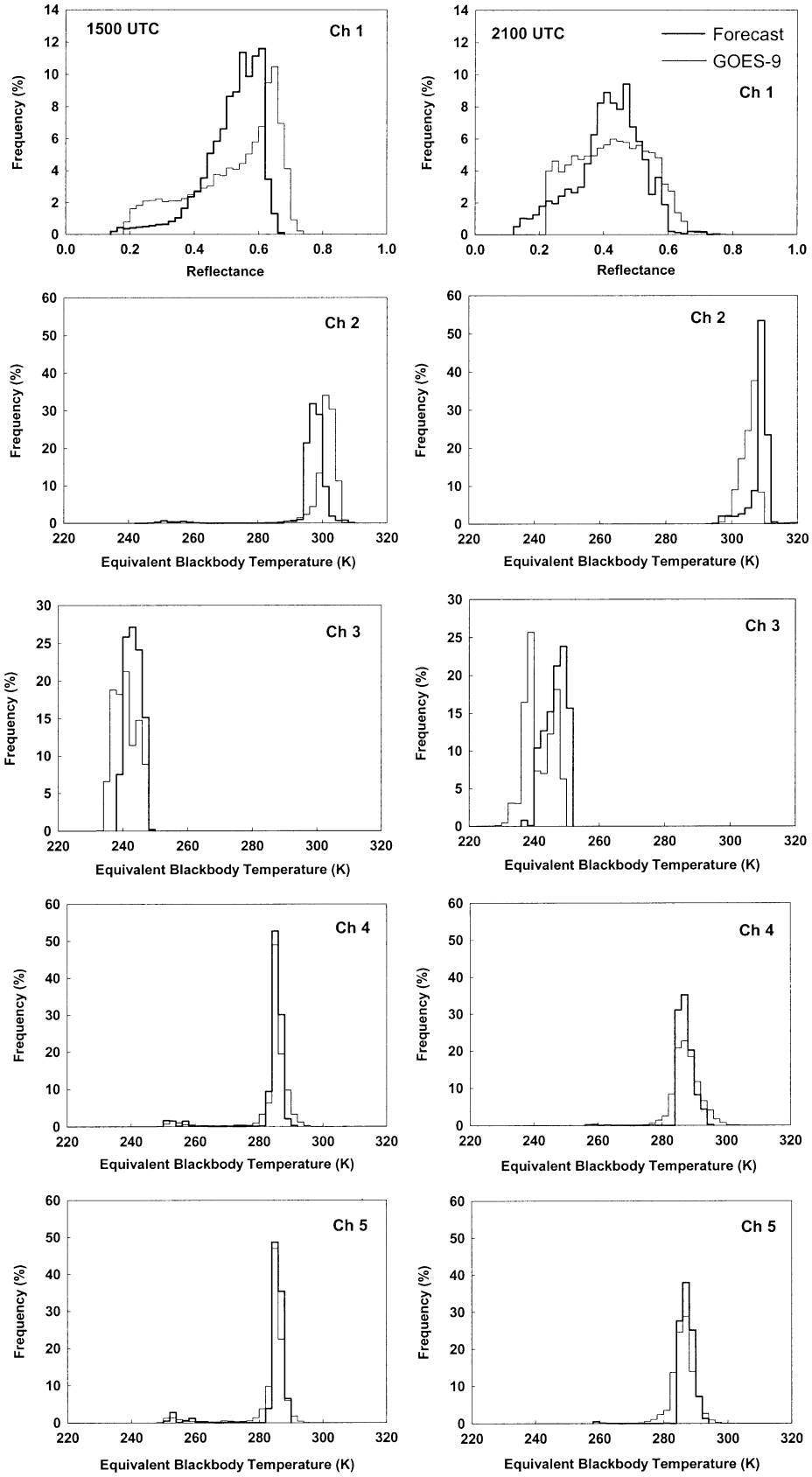

FIG. 10. Frequency distributions of cloudy radiances for data in Fig. 9.

suitable for practical use in data assimilation for mesoscale models containing explicit microphysics. Although it may be used for computing both clear and cloudy radiances, emphasis in this study was given to the cloudy case. Special features unique to this operator include

- RT models that account for multiple scattering,
- rapid calculation of cloudy radiances, even at visible wavelengths,
- general applicability to many types of narrowband satellite sensors,
- use of physical models that allows straightforward calculations of optical properties for any number of hydrometeor types. Models include a new application of anomalous diffraction theory to compute asymmetry factor.

The observational operator, however, has some limitations that deserve mention. For instance, the ADT model for computing the asymmetry factor performs poorly at visible wavelengths and thus either improvements to the model are required or an alternative parameterization, such as outlined in appendix B, must be used. The ADT asymmetry factor model is also somewhat computationally inefficient and may require further modifications to be useful in an operational setting. Also, the Henyey–Greenstein scattering phase function used to approximate the Lorenz–Mie phase function was found to produce errors as high as about 20% in special cases. While not negligible, these errors are deemed acceptable given the even larger uncertainties due to cloud brokenness in addition to forecast errors in the cloud microphysics.

The observational operator was tested by forecasting a continental stratus system with RAMS and computing radiances at GOES imager wavelengths. At both 15- and 21-h forecast periods, the predicted cloudy radiances compared very well quantitatively to *GOES-9* imager measurements at all five channels. Most importantly, the coupled observational operator–RAMS system was able to reproduce subtle *temporal* changes that occurred in the distribution of cloudy radiances between the two verification periods. This ability is a crucial element in any 4DVAR data assimilation.

While the fidelity of the mesoscale model and the observational operator play key roles in producing reasonable cloudy radiances, other factors, such as the phenomenon being predicted and the wavelength of the observation, are important. Clearly in this case, success was achieved because of RAMS's skill in forecasting cloud mixing ratio (in terms of both magnitude and location) and the validity of the approximations assumed in the cloud optical property and RT modeling. Accurate prediction of cloud mixing ratio is important for computing radiances in window regions (e.g., 0.63, 3.92, and 10.7 μm) because radiances have a strong to moderate sensitivity to this quantity, whereas accurate prediction of vapor mixing ratio and/or temperature are more important for radiances in regions of strong molecular absorption (e.g., 6.77 μm). Other diagnostic microphysical quantities, such as the size distribution width, have a smaller, second-order effect on cloudy radiances in most parts of the spectrum and thus may be specified a priori. It was also demonstrated that near-IR radiance (3.92 μm) calculations are fairly sensitive to changes in the droplet number concentration. Therefore, microphysical schemes that do not predict number concentration for water droplets (as in this study) may limit the usefulness of these measurements in data assimilation because they do not allow the forecast model to fully exploit the information content of the measurements.

The most challenging part of implementing the observational operator in a 4DVAR assimilation system will be in developing its adjoint, which provides the necessary gradient information. This work is in progress. There are also plans to extend the observational operator to include the microwave spectrum as well, measurements that provide unique information on the atmospheric and surface water components. We anticipate that when satellite radiance measurements across the full spectrum are combined and used within a mesoscale model 4DVAR data assimilation system, not only will cloud forecasts improve but also prediction of all other parts of the atmospheric water budget.

Acknowledgments. This work was supported by the DOD Center for Geosciences/Atmospheric Research Grant DAAL01-98-2-0078. We greatly appreciate the efforts of Tom Kleespies in providing the OPTRAN code and error statistics and for deriving the coefficients for *GOES-9* imager channel 1. Thanks also go to Cindy Combs for her assistance with the regression analysis. The surface microwave radiometer data and rawinsonde data at Morris, Oklahoma, were obtained from the ARM Program sponsored by the United States Department of Energy, Office of Energy Research, Office of Health and Environmental Sciences Division. We also thank John Lewis whose comments helped to improve the paper.

APPENDIX A

Formulation of Asymmetry Factor from Anomalous Diffraction Theory

The phase function from anomalous diffraction theory integrated over the gamma distribution is

$$P(\Theta) = \frac{N_o}{Q_{\text{sca}}}\left(\frac{\pi}{2\lambda}\right)^2 \int_0^\infty |A(D, \Theta)|^2 D^{4+\nu} e^{-\Lambda D}\, dD, \quad \text{(A1)}$$

where Q_{sca} is the scattering efficiency, D is particle diameter, λ is the wavelength of incident radiation, and the complex amplitude function (van de Hulst 1981) that includes particle absorption is

$$A(D, \Theta) = \int_0^{\pi/2} (1 - e^{-\rho(i+\tan\beta)\sin\tau}) J_0(z\cos\tau)\cos\tau\sin\tau\, d\tau, \quad \text{(A2)}$$

where $\rho = 2x(n_r - 1)$, $x = \pi D/\lambda$, $\tan\beta = n_i/(n_r - 1)$, $z = x\Theta$, J_0 is the zeroth order Bessel function, and n_r and n_i are the real and imaginary parts, respectively, of the complex refractive index of the particle. Using (A1), the asymmetry factor follows as

$$g = \int_{-1}^{1} P(\mu)\mu\, d\mu, \quad \text{(A3)}$$

where $\mu = \cos(\Theta)$. Because these series of integrals have no known solution, the disadvantage of this approach is that it becomes somewhat numerically cumbersome to compute g. Through trial and error it was found that the best compromise between accuracy and speed was to use 56-point Gauss–Legendre quadrature for solving the integral in (A2), 32 points in (A1) over the size range 0–200 μm, and 24 points in (A3).

APPENDIX B

Asymmetry Factor Parameterization

A simple parameterization is given for predicting the asymmetry factor g for the visible channel of the GOES imager. First, tables of the asymmetry factor were created from Lorenz–Mie calculations for droplet effective radius (r_e) ranging from 2 to 35 μm in 1-μm increments and gamma distribution width parameter (ν) from 2 to 30 in increments of 2 at selected wavelengths. Mean values of g across the instrument bandpass were weighted by the instrument's response and the solar spectrum. A Hill-type function was found to provide the best fit to the asymmetry factor over a wide range of r_e:

$$g = \left[\frac{\alpha r_e^{\beta}}{\gamma^{\beta} + r_e^{\beta}}\right],$$

where r_e is in μm and α, β, and γ are functions of ν as

$$\alpha = a_1 + a_2 \exp\left\{-\frac{1}{2}\left[\frac{1}{a_3}\ln\left(\frac{\nu}{a_4}\right)\right]^2\right\}$$

$$\beta = b_1 + b_2 \exp\left\{-\frac{1}{2}\left[\frac{1}{b_3}\ln\left(\frac{\nu}{b_4}\right)\right]^2\right\}$$

$$\gamma = \frac{\gamma_1 + \gamma_2\nu + \gamma_3\nu^2}{1 + \gamma_4\nu + \gamma_5\nu^2}$$

and $a_1 = -0.0027$, $a_2 = 0.9559$, $a_3 = 6.4924$, $a_4 = 0.88627$, $b_1 = 0.1148$, $b_2 = 0.9409$, $b_3 = 6.4131$, $b_4 = 0.7682$, $\gamma_1 = 0.0971$, $\gamma_2 = 0.0258$, $\gamma_3 = 0.0018$, $\gamma_4 = 0.0214$, and $\gamma_5 = 0.0249$, which were obtained from least squares regression. Errors were less than 5% for the full range of conditions.

REFERENCES

Bayler, G. M., R. M. Aune, and W. H. Raymond, 2000: NWP cloud initialization using GOES sounder data and improved modeling of nonprecipitating clouds. *Mon. Wea. Rev.*, **128,** 3911–3920.

Bremer, J. C., J. G. Baucom, H. Vu, M. P. Weinreb, and N. Pinkine, 1998: Estimation of long-term throughput degradation of GOES-8 and -9 visible channels by statistical analysis of star measurements. *Proc. SPIE Conf. on Earth Observing Systems III*, San Diego, CA, SPIE, 145–149.

Deeter, M., and K. F. Evans, 1998: A hybrid Eddington-single scattering radiative transfer model for computing radiances from thermally emitting atmospheres. *Quart. J. Roy. Meteor. Soc.*, **60,** 635–648.

Derber, J. C., and W.-S. Wu, 1998: The use of TOVS cloud-cleared radiances in the NCEP SSI analysis system. *Mon. Wea. Rev.*, **126,** 2287–2299.

English, S. J., R. J. Renshaw, P. C. Dibben, A. J. Smith, P. J. Rayer, C. Poulsen, F. W. Saunders, and J. R. Eyre, 2000: A comparison of the impact of TOVS and ATOVS satellite sounding data on the accuracy of numerical weather forecasts. *J. Quant. Spectrosc. Radiat. Transfer*, **126,** 2911–2931.

Evans, K. F., 1998: The spherical harmonics discrete ordinate method for three-dimensional atmospheric radiative transfer. *J. Atmos. Sci.*, **55,** 429–446.

Eyre, J. R., 1987: On systematic errors in satellite sounding products and their climatological mean values. *Quart. J. Roy. Meteor. Soc.*, **113,** 279–292.

——, G. A. Kelly, A. P. McNally, E. Andersson, and A. Persson, 1993: Assimilation of TOVS radiance information through one-dimensional variational analysis. *Quart. J. Roy. Meteor. Soc.*, **119,** 1427–1463.

Feingold, G., B. Stevens, W. R. Cotton, and A. S. Frisch, 1996: On the relationship between drop in-cloud residence time and drizzle production in stratocumulus clouds. *J. Atmos. Sci.*, **53,** 1108–1122.

Grant, I. P., and G. E. Hunt, 1969: Discrete space theory of radiative transfer I. Fundamentals. *Proc. Roy. Soc. London*, **313,** 183–197.

Harrington, J. Y., 1997: The effects of radiative and microphysical processes on simulated warm and transition season Arctic stratus. Ph.D. dissertation, Colorado State University, 289 pp. [Available from Colorado State University, Dept. of Atmospheric Science, Fort Collins, CO 80523.]

——, G. Feingold, and W. R. Cotton, 2000: Radiative impacts on the growth of a population of drops within simulated summertime arctic stratus. *J. Atmos. Sci.*, **57,** 766–785.

Knapp, K. R., and T. H. Vonder Haar, 2000: Calibration of the Eighth Geostationary Observational Environmental Satellite (*GOES-8*) imager visible sensor. *J. Atmos. Oceanic Technol.*, **17,** 1639–1644.

McMillin, L. M., L. J. Crone, M. D. Goldberg, and T. J. Kleespies, 1995a: Atmospheric transmittance of an absorbing gas, 4. OPTRAN: A computationally fast and accurate transmittance model for absorbing gases with fixed and variable mixing ratios at variable viewing angles. *Appl. Opt.*, **34,** 6269–6274.

——, ——, and T. J. Kleespies, 1995b: Atmospheric transmittance of an absorbing gas, 5. Improvements to the OPTRAN approach. *Appl. Opt.*, **34,** 8396–8399.

Menzel, W. P., and J. F. W. Purdom, 1994: Introducing GOES-I: The first in a new generation of geostationary operational satellites. *Bull. Amer. Meteor. Soc.*, **75,** 757–780.

Meyers, M. P., R. L. Walko, J. Y. Harrington, and W. R. Cotton, 1997: New RAMS cloud microphysics parameterization. Part II: The two-moment scheme. *Atmos. Res.*, **45,** 3–39.

Miles, N. L., J. Verlinde, and E. E. Clothiaux, 2000: Cloud droplet

size distributions in low-level stratiform clouds. *J. Atmos. Sci.,* **57,** 295–311.

Mitchell, D. L., 1996: Use of mass- and area-dimensional power laws for determining precipitation particle terminal velocities. *J. Atmos. Sci.,* **53,** 1710–1723.

——, 2000: Parameterization of the MIE extinction and absorption coefficients for water clouds. *J. Atmos. Sci.,* **57,** 1311–1326.

Pielke, R. A., and Coauthors, 1992: A comprehensive modeling system—RAMS. *Meteor. Atmos. Phys.,* **49,** 69–91.

——, M. E. Nicholls, R. L. Walko, J. A. Nygaard, and X. Zeng, 1997: Several unresolved issues in numerical modeling of geophysical flows. *Numerical Methods in Atmospheric and Oceanic Modelling: The André J. Robert Memorial Volume,* C. Lin, R. Caprise, and H. Ritchie, Eds., Canadian Meteorological and Oceanographic Society/NRC Research Press, 557–581.

Smith, W. L., Jr., P. Minnis, D. F. Young, and Y. Chen, 1999: Satellite-derived land surface emissivity for ARM and CERES. Preprints, *10th Conf. on Atmospheric Radiation,* Madison, WI, Amer. Meteor. Soc., 409–412.

Soden, B., and Coauthors, 2000: An intercomparison of radiation codes for retrieving upper-tropospheric humidity in the 6.3-μm band: A report from the first GVaP workshop. *Bull. Amer. Meteor. Soc.,* **81,** 797–808.

Stamnes, K., and R. A. Swanson, 1981: New look at the discrete ordinate method for radiative transfer calculations in anisotropically scattering atmospheres. *J. Atmos. Sci.,* **38,** 387–399.

Sun-Mack, S., Y. Chan, T. D. Murray, P. Minnis, and D. F. Young, 1999: Visible clear-sky and near-infrared surface albedos derived from VIRS data for CERES. *10th Conf. on Atmospheric Radiation,* Madison, WI, Amer. Meteor. Soc., 422–429.

Tripoli, G. J., 1986: A numerical investigation of an orogenic mesoscale convective system. Ph.D. dissertation, Dept. of Atmospheric Science Paper 401, Colorado State University, Fort Collins, CO, 290 pp.

——, and W. R. Cotton, 1982: The Colorado State University three-dimensional cloud/mesoscale model—Part I General theoretical framework and sensitivity experiments. *J. Rech. Atmos.,* **16,** 185–219.

van de Hulst, H. C., 1981: *Light Scattering by Small Particles.* Dover, 470 pp.

Vukićević, T., T. Greenwald, R. Hertenstein, and M. Ghemires, 2001: Use of cloudy radiance observations in mesoscale data assimilation. *Proc. Fifth Symp. on Integrated Observing Systems,* Albuquerque, NM, Amer. Meteor. Soc., 113–117.

Walko, R. L., W. R. Cotton, M. P. Meyers, and J. Y. Harrington, 1995: New RAMS cloud microphysics parameterization Part I: The single moment scheme. *Atmos. Res.,* **38,** 29–62.

Wiscombe, W. J., 1976: On initialization, error and flux conservation in the doubling method. *J. Quant. Spectrosc. Radiat. Transfer,* **16,** 637–658.

——, 1977: Delta-M method: Rapid yet accurate radiative flux calculations for strongly asymmetric phase functions. *J. Atmos. Sci.,* **34,** 1408–1422.